UC San Diego

UC San Diego Previously Published Works

Title

Investigating the conformational dynamics of SARS-CoV-2 NSP6 protein with emphasis on non-transmembrane 91-112 & 231-290 regions.

Permalink

Journal

Authors

Kumar, Amit
Kumar, Prateek
Saumya, Kumar
et al.

Publication Date

DOI

Peer reviewed

Investigating the conformational dynamics of SARS-CoV-2 NSP6 protein with emphasis on non-transmembrane 91–112 & 231–290 regions

Amit Kumar, Prateek Kumar, Kumar Udit Saumya, Rajanish Giri[*]

School of Basic Sciences, Indian Institute of Technology Mandi, VPO Kamand, Himachal Pradesh, 175005, India

ABSTRACT

The NSP6 protein of SARS-CoV-2 is a transmembrane protein, with some regions lying outside the membrane. Besides a brief role of NSP6 in autophagosome formation, this is not studied significantly. Also, there is no structural information available to date. Based on the prediction by TMHMM server for transmembrane prediction, it is found that the N-terminal residues (1-11), middle region residues (91–112), and C-terminal residues (231–290) lies outside the membrane. Molecular Dynamics (MD) simulations showed that NSP6 consists of helical structures. In contrast, the membrane outside lying region (91–112) showed partial helicity, which was further used as a model and obtained disordered type conformation during 1.5 μs. Additionally, a 200ns simulation study of residues 231–290 have shown significant conformational changes. As compared to helical and beta-sheet conformations in its structure model, the 200ns simulation resulted in the loss of beta-sheet structures while helical regions remained intact. Further, we have experimentally characterized the residue 91–112 by using reductionist approaches. CD spectroscopy suggests that the NSP6 (91–112) is disordered-like region in isolation, which gains helical conformation in different biological mimic environmental conditions. These studies can be helpful to study NSP6 (91–112) interactions with host proteins, where different protein conformations might play a significant role. The present study adds up more information about the NSP6 protein aspect, which could be exploited for its host protein interaction and pathogenesis.

1. Introduction

Severe acute respiratory syndrome-coronavirus 2 (SARS-CoV-2) has positive-sense single-stranded RNA genomes (~30 kilobases), which encodes sixteen non-structural proteins [1]. Numerous articles describe the SARS-CoV-2 life cycle, genome, proteome, and functioning mechanisms [2–5]. Among non-structural proteins (NSPs), significantly less is known about NSP6, specifically, there is no 3D structure available to date. Gordon et al. stated that NSP6 interacts with host proteins, although the mechanism remains elusive [4]. A yeast two-hybrid assays shows that NSP6 interacts with other non-structural viral proteins of SARS-CoV [6]. The information on NSP6 protein is minimal such as structural studies, host protein interactions, and many other, which are still needed to address. It is reported that NSP6 protein is a six-pass membrane-spanning protein facing its both terminal at the cytosolic side [7–9]. The NSP6 protein, along with NSP3 and NSP4, forms a double-membrane vesicle [10].

The coronaviruses (CoV-1 and CoV-2) NSP6 protein interacts with sigma receptor 1 (*SIGMAR1*) [4]. Further, it is seen for CoV-1 NSP6 that

it plays a role in autophagy, even in the absence of its C-terminal region [8]. Considering the NSP6 interaction with host proteins, the structural characterization of either full length or partial NSP6 domain is necessary to understand the SARS-CoV-2 pathogenicity mechanism. However, the surrounding environment plays an essential role in the conformational dynamics of protein or its interacting regions [11]. The change in conformation is governed by the covalent (i.e., phosphorylation, ubiquitination) and/or non-covalent events i.e., binding of ions, lipids, drugs, proteins etc., and environmental influences such as macromolecular crowding, osmolyte, pH, and temperature [11–16]. Factors influencing the change in protein's conformational dynamics ultimately decide the fate of subsequent protein signaling events [11,17].

In the present study, we have used TMHMM server to predict the regions lying outside the membrane to potentially interact with host proteins. We have characterized NSP6 full length, membrane outside lying region of NSP6 and NSP6–C terminal region (CTR) based on computational modeling and simulation. Further, we experimentally characterized the synthetic peptide corresponding residues 91–112 (which lies outside the membrane region) and studied in isolation for its
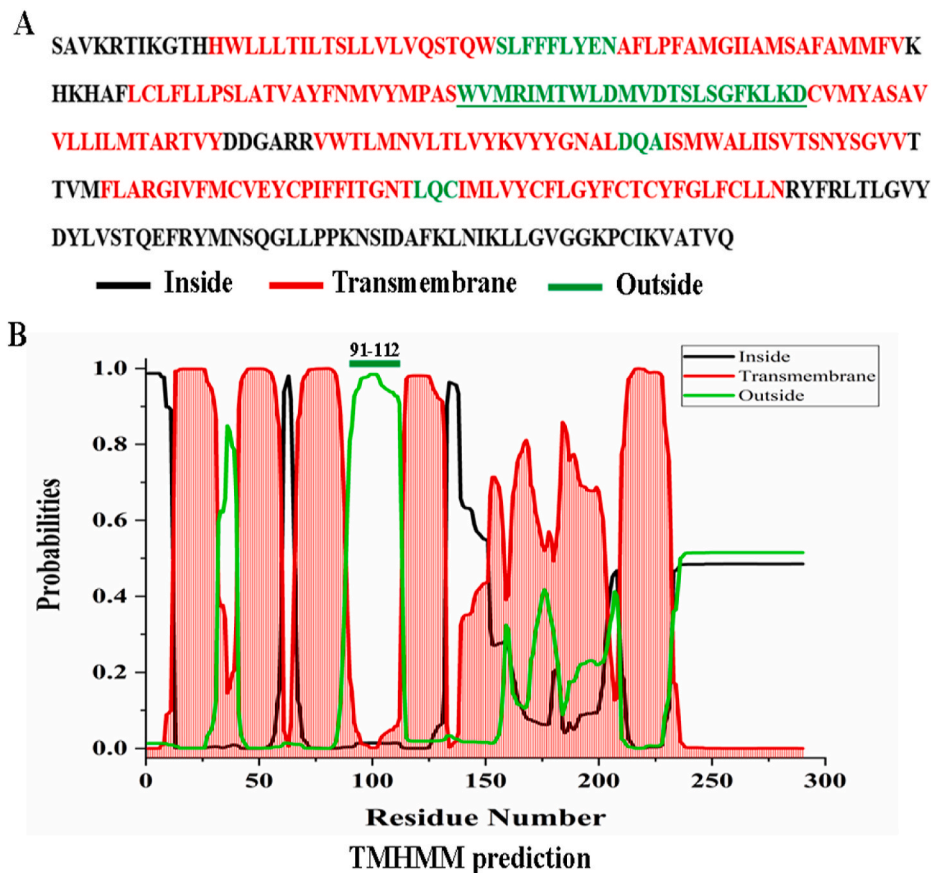
Fig. 1. (A) The primary sequence of SARS CoV-2 NSP6 full length with color pattern showing the inside, outside and transmembrane regions. (B) TMHMM server prediction with color pattern showing the residue 91–112 lies outside the membrane.

conformational dynamics to validate our computational simulations. The short peptide sequence gives invaluable information regarding their conformation in their capabilities to regulate the cellular process or in the context of complete global structure [18,19]. Our studies found that this region is disordered like in isolation and gain helical conformation in the presence of TFE and SDS, which may suggest its propensity to gain structure while interacting with its potential partners.

2. Material and methods

2.1. Chemicals and reagents

The NSP6 peptide (residues 91–112) "-NH2-VMRIMTWLDMVDTSLSGFKLKD–COOH–", with purity >88% was purchased from Gene script, USA. Organic solvents such as Trifluoroethanol (TFE) with ≥99% purity was purchased from Sigma-Aldrich. Lyophilized peptide was dissolved in 10 mM sodium phosphate buffer (pH 7.0) at a concentration of 10 μM.

### 2.2. Topology prediction of NSP6 protein

Prediction of transmembrane segments was done using TMHMM [20], MEMSAT-SVM [21], and CCTOP servers [22] using default parameters.

2.3. Molecular dynamics (MD) simulation

We have utilized I-TASSER, PepFold, and RaptorX [23–25] web-servers for constructing the 3D models for the NSP6 full-length (NSP6-FL), NSP6 (residues 91–112) and NSP6-CTR, respectively. The resultant models were then prepared using Chimera by adding missing hydrogens and missing sidechains were completed in residues [26]. We have utilized Charmm36m forcefield in Gromacs v5 on high-performance cluster (HPC) of IIT Mandi, where simulation setup was built by placing the protein structure (NSP6 91–112 and NSP6-CTR) in a cubic box with a distance of 10 Å from each edge along with SPC water model and 0.15 M NaCl salt concentration. NSP6 is a membrane bound protein, therefore for full length NSP6 model lipid membrane environment was provided. The simulation setup for NSP6 full-length was built using CHARMM-GUI web server, where 250 molecules of neutrally charged lipid, Dioleoylphosphatidylcholine (DOPC) [27] around the predicted transmembrane regions were placed. Those regions are residues 12–31, 41–60, 67–89, 113–132, 139–158, 162–179, 184–206, 210–232 which encompasses the whole protein except few outlier regions with dimensions 99.01, 99.01, 104.86 Å of a rectangular box. After solvation, all systems were charge neutralized with counterions. The steepest descent method was used to attain an energy minimized simulation system until the system was converged within 1000 kJ/mol. Further, the equilibration of the system was done to optimize solvent in the environment. Using NVT and NPT ensembles within periodic boundary conditions for 100ps each, the system was equilibrated. The average temperature at 300K and pressure at 1 bar were maintained using Nose-Hoover and Parrinello-Rahman coupling methods during the simulation. All bond-related constraints were solved using SHAKE algorithm. The final production run was performed for 100ns, 1500ns (1.5 μs), and 200ns, for NSP6-FL, NSP6 (91–112), and NSP6-CTR, respectively.

All trajectory analysis calculations and visualizations were performed using Chimera, maestro, vmd and Gromacs command for calculating the helicity, root mean square deviation (RMSD), root mean
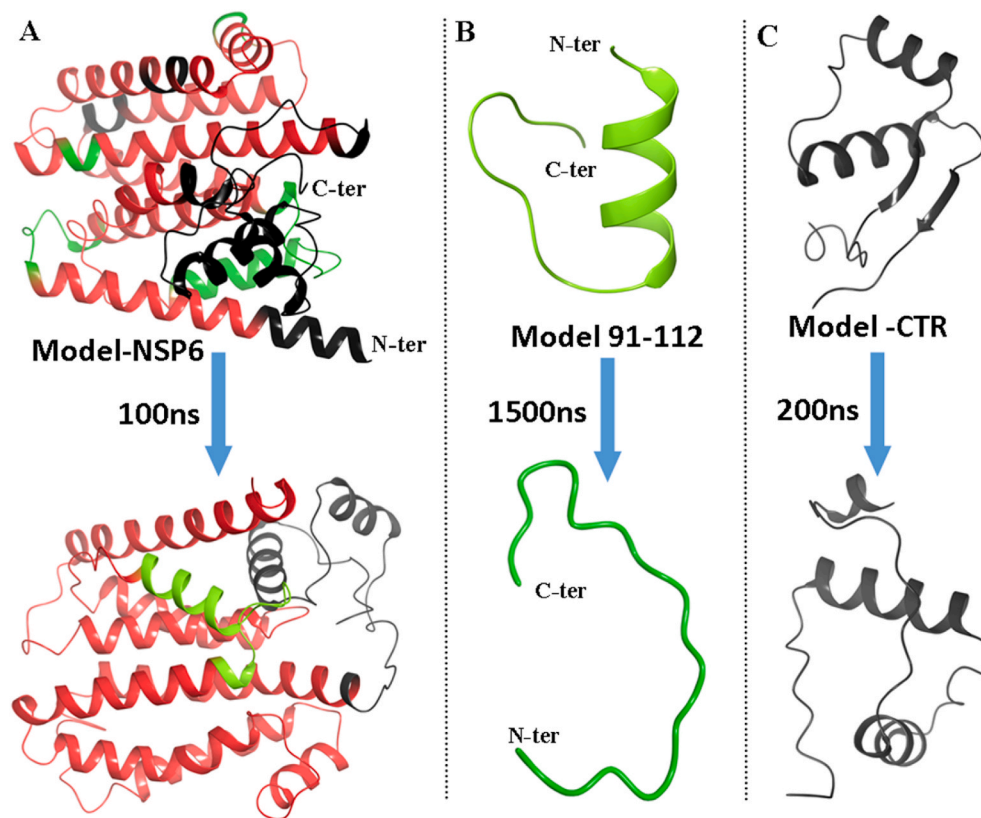
Fig. 2. (A) Model of the full-length NSP6 build from I-TASSER server as no 3D structure available till date and simulated for 100ns. (B) The NSP6 residues 91–112 in isolation showed random coil after simulation for 1.5 μs of the 3D model built from PepFold server. (C) The NSP6-CTR model corresponding to residues 231–290 built using RaptorX webserver shows only helical conformation after 200ns. The color pattern in protein models is showing the inside (Black), outside (Green), and transmembrane region (Red).

square fluctuation (RMSF), and radius of gyration (Rg).

2.4. Liposome preparation

The liposomes were prepared, as described earlier [15]. Briefly, the negatively charged lipid DOPS (1,2-dioleoyl-sn-glycer-o-3-phospho-ʟ-serine) was purchased from Avanti Polar Lipids (Alabaster, AL). The chloroform from the lipid solution was removed using a rotary evaporator at 40 °C, and the dry lipid films were hydrated in 50 mM phosphate buffer (pH 7.4). The final concentration of the DOPS liposomes was 24.69 mM. The resulting suspension was freeze-thaw-vortex in liquid nitrogen and water at 60 °C, following which the lipids were extruded 25 times through the mini extruder (Avanti Polar Lipids, Inc. USA) through cut off filter of 100 nm polycarbonate membrane to prepare uniform Large unilamellar vesicles (LUV).

2.5. Circular dichroism spectroscopy

JASCO machine (Jasco J-1500 CD spectrometer) was used for CD data recording. 5 μM peptide sample were prepared in 10 mM phosphate buffer, pH 7.0. The peptide was kept in organic solvents (TFE) with increasing concentration from 0 to 50%, and far-UV (190–240 nm) spectra were recorded in 1 mm quartz cuvette. Similarly, the peptide (10 μM) was assessed for structural changes in Sodium Dodecyl Sulfate (SDS) and liposome DOPS. Similarly, the peptide was assessed for structural changes under the effect of increasing temperature from 10 to 90 °C. All the spectra were recorded at a scan speed of 50 nm/min with a response time of 1s and 1 nm bandwidth and three technical repeats. The equivalent spectra of buffers were recorded and subtracted from the spectra of the test samples. Further, the smoothing of CD spectra was done by Savitsky-Golay fitting at 5 points of smoothing window and second polynomial order.

2.6. Fluorescence spectroscopy

We monitored the intrinsic Trp fluorescence intensity in NSP6 (91–112). A 5 μM peptide in 10 mM sodium phosphate buffer (pH 7.0) was prepared with increasing TFE and SDS concentration. Emission spectra were recorded from 300 to 500 nm at 295 nm excitation wavelength in a Horiba Fluorolog-3 spectrofluorometer. The individual negative blank was subtracted from each test sample [14].

3. Results and discussion

3.1. TMHMM server predicted NSP6 (residues 91–112) lies outside the membrane

Firstly, we have predicted the topology of NSP6 protein with the help of several protein topology prediction algorithms. The TMHMM server, a consensus server CCTOP, and MEMSET server were used to characterize the amino acid of NSP6 for their transmembrane region, inside and outside of membrane region (Fig. 1A & B, Supplementary Fig. 1). Similarly, Benvenuto et al. showed seven transmembrane regions in NSP6 of coronaviruses by using TMHMM server and investigated the effect of mutation in NSPs and orf10 in their adjacent region [7]. Recently, SARS-CoV-2 E protein topology has been predicted and experimentally validated with the help of these servers [28,29].

3.2. MD simulations of full-length NSP6, NSP6 (91–112) and NSP-CTR

We have built the 3D model of full-length NSP6, NSP6 C-terminal region (CTR), and NSP6 (residues 91–112). Firstly, the model built using different web servers was simulated for appropriate simulation time. As shown in Fig. 2, the NSP6-FL comprised multiple helical regions, which were predicted to be transmembrane region (shown in red; Fig. 2A), outside membrane regions (shown in green; residues 91–112; Fig. 2B), and inside membrane region (shown in black; residues 231–290;
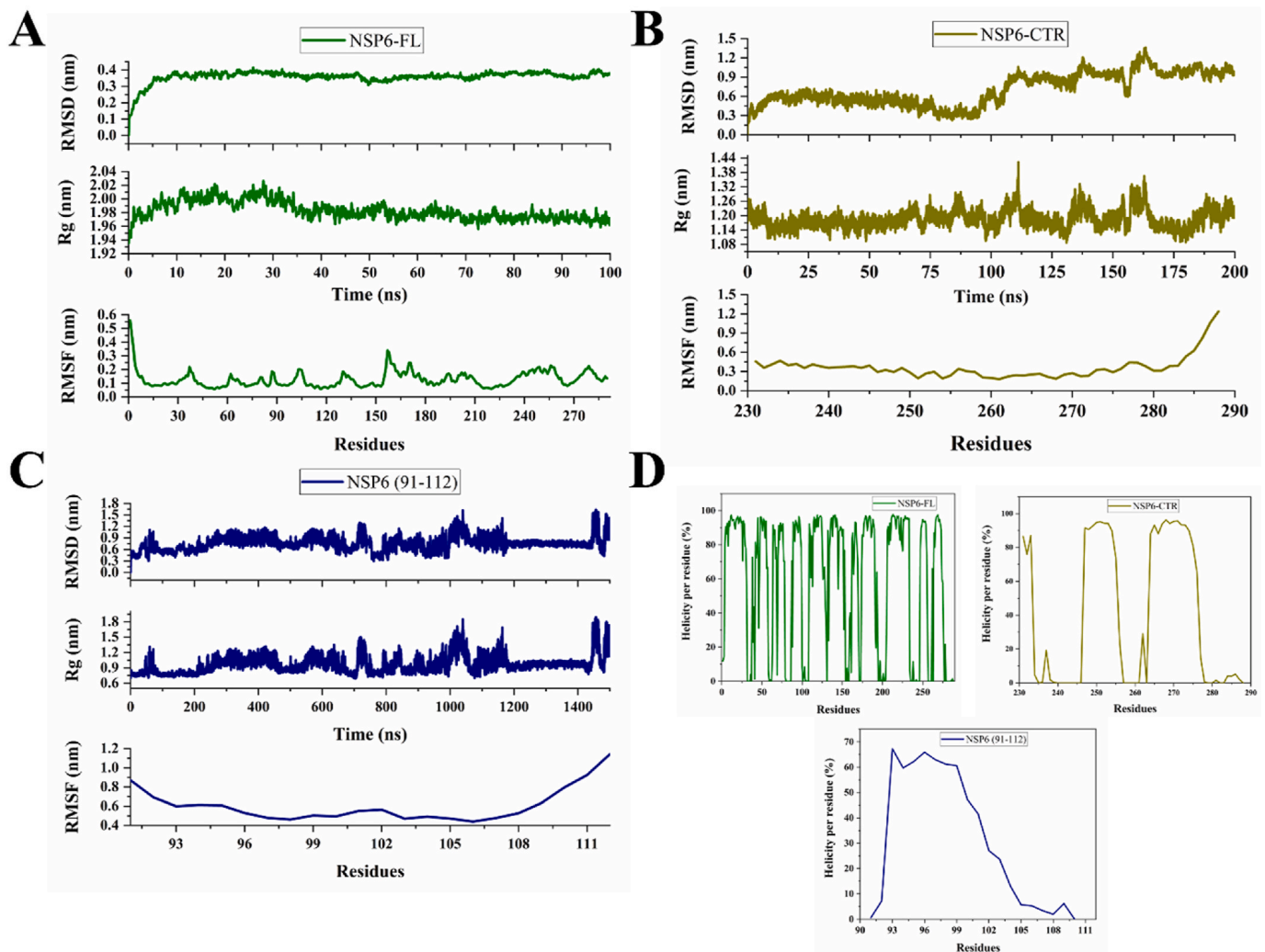
Fig. 3. Molecular Dynamics Simulation analysis based on Root Mean Square Deviation (RMSD), Radius of gyration (Rg), and Root Mean Square Fluctuations (RMSF) of Model NSP6 full-length (A), NSP6 (residues 91–112) (B), NSP6-CTR region (residues 231–290) (C). In figure (D), the helicity percentage over throughout the simulation period is shown for all three simulated structures.

Fig. 2C). After 100 ns of MD simulations of NSP6-FL, the membrane passing helical regions were intact. In contrast, the regions lying outside the membrane showed fewer changes in secondary structure (secondary structure timeline is shown in Supplementary Fig. 1). In isolation, the structure model of residues 91–112 consisted of nearly 65% of the helix in its structure but has shown substantial structural changes after simulations. The NSP6 (residues 91–112) lost its helicity after 1.5 μs, which showed its disorder character in isolation (Fig. 2B). This is also confirmed from secondary structure timeline shown in Supplementary Fig. 2. Interestingly, the C-terminal or cytosolic region (residues 231–290) is predicted to comprise both helical and beta sheets ($_{243}$DYL$_{245}$ and $_{283}$CIK$_{285}$) conformations in its structure model built using RaptorX. Upon simulating it for 200 ns, the beta-sheet structures of the NSP6-CTR region have converted to loop regions. Additionally, the helical regions were intact upto 200ns (secondary structure timeline is shown in Supplementary Fig. 3).

Further, we have analyzed the time-dependent simulation frame analyses through Root Mean Square Deviation (RMSD), Radius of gyration (Rg), and Root Mean Square Fluctuation (RMSF) values (Fig. 3). First, the modeled structure of NSP6 was simulated in the presence of a membrane to check its conformation. Its RMSD values deviated initially (up to 0.35 nm till 10ns approx.) and then stabilized at 0.35 nm after that upto the entire simulation time. These trends were also reflected in the Rg time-dependent parameters, where values fluctuated up to 40ns

and stabilized thereafter. According to RMSF trend, the N-terminals residues fluctuate heavily. The middle regions and residue nearby to CTR also showed fluctuation (Fig. 3B). Finally, the average helicity calculation for 100 ns simulation has shown an intact helix with >90% for the majority of the helices except for small helices, which have shown minor fluctuations (Fig. 3D).

Next, the inside membrane region of NSP6 (NSP6-CTR) has shown a stable trend in RMSD and Rg in initial 90 ns with an approx. Average RMSD of 0.45 nm and Rg of 1.18 nm (Fig. 3B). Afterward, the fluctuations were increased in mean distances, which may be due to a change in the structure of NSP6-CTR, mainly due to the transition of beta-sheets to coil. The average RMSF of NSP6-CTR is in the favorable range, with minimal fluctuations in some residues.

The modeled structure of NSP6 (91–112) was simulated in water as it lies outer surface as per predictions. The RMSD, Rg values were found deviating upto 1200ns and stabilized thereafter. According to RMSF trend, except the residues 96–99 and residues 102–105, other residues fluctuate heavily (Fig. 3C). The change in structural regions is also evident from Fig. 3D, where the helicity has declined from nearly 70% for residues 93–102. This claim is further investigated using synthesized peptide based spectroscopic studies.

Recently, atomistic-level studies using microseconds long MD simulations provide insight into important residues responsible for the high-affinity interaction among spike protein with ACE receptors of SARS-
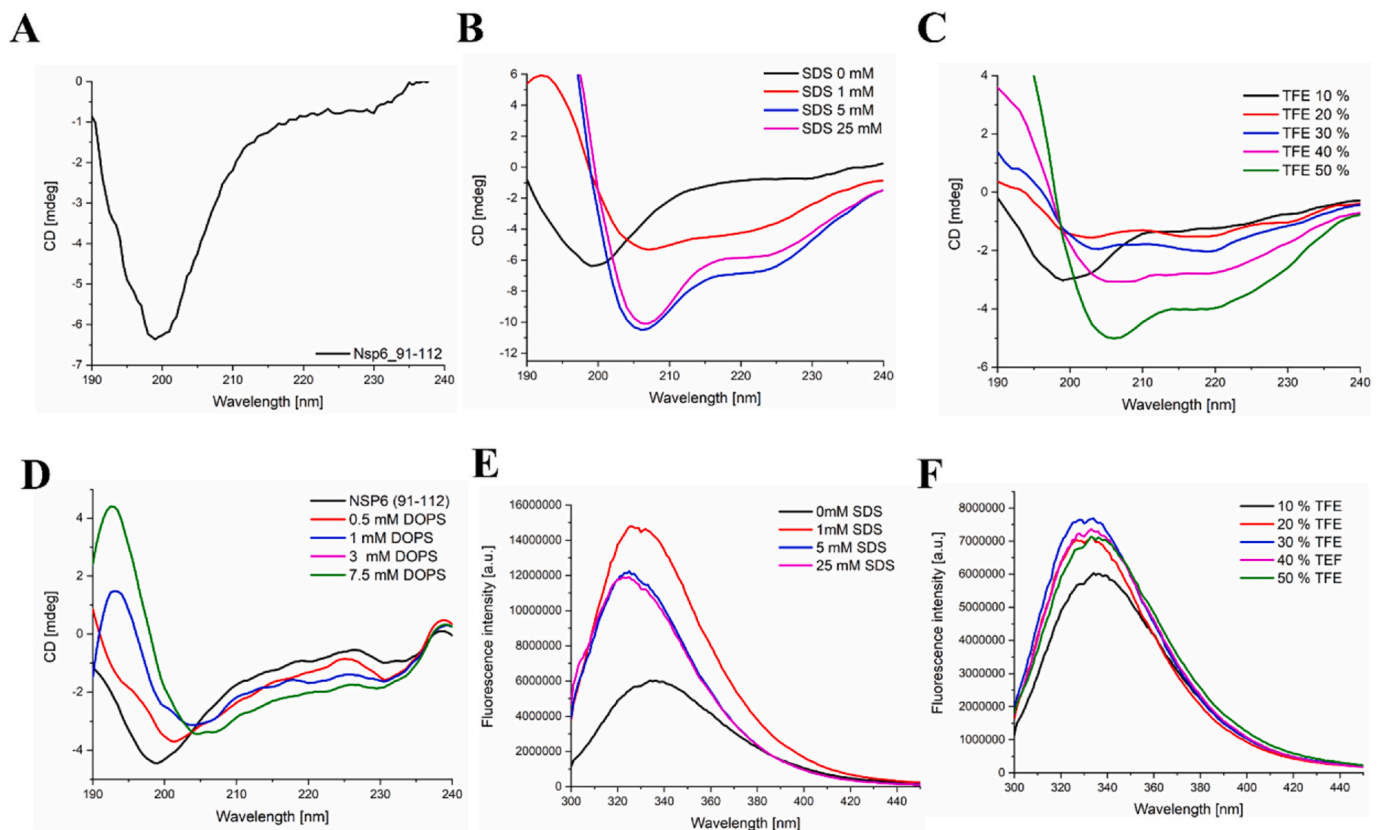
Fig. 4. Conformation of NSP6 (91–112) studied with CD and fluorescence spectroscopy. (A) NSP6 91–112 region showed negative ellipticity under physiological pH buffer conditions. In the presence of SDS (B) and TFE (C) peptide gained helical conformation at 208 nm and 222 nm. (D) The negatively charged liposome DOPS induces partial helical conformation in the peptide. Fluorescence spectroscopy showed tertiary structural changes in the NSP6 91–112 region. In the presence of SDS (E) and TFE (F) peptide showed significant blue shift under the influence of hydrophobic environment.

CoV-2 using by creating a residue-residue contact map using simulation trajectories [30]. Further, an unbiased MD simulation study of fully glycosylated spike protein reveals the essential information about immunogenic regions using long timescale MD simulations [31]. As thoroughly reviewed by Serapian and Colombo, the protein-protein interaction using direct or allosteric sites describe their importance to be targeted using small molecules which may disrupt their functions [32]. Therefore, in light of the detailed atomistic level study of NSP6 and its subdomain, it might be pivotal to unravel some characteristic feature of this protein for the epitope determination or to explain the molecular trait responsible for protein-protein interactions. The structural dynamics of NSP6 described here can also be useful to decipher strategies for using it as a therapeutic target.
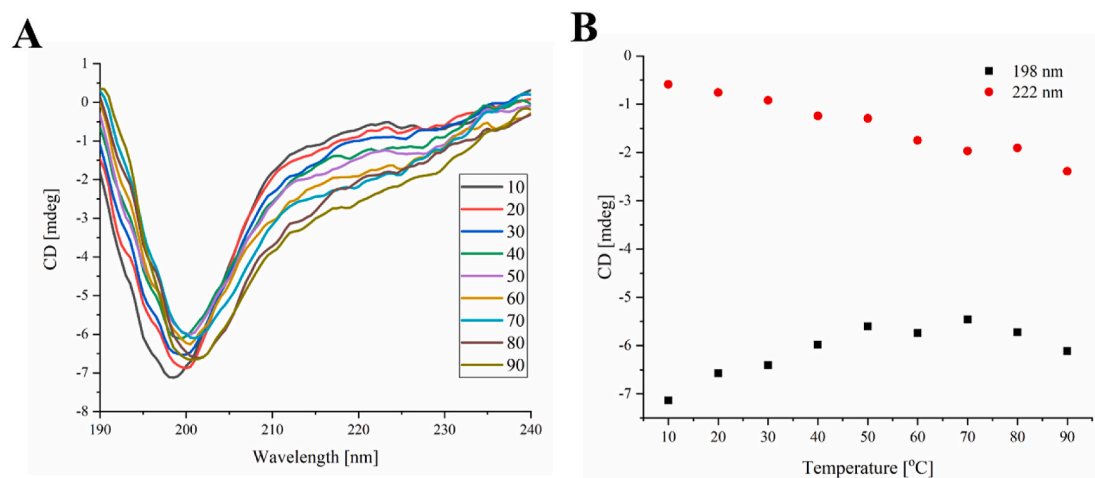
Fig. 5. Temperature-induced structural changes in NSP6 (90–112). (A) At higher temperatures negative ellipticity was observed at 222 nm shows gain in a helical conformation. (B) Negative ellipticity at 198 nm and 222 nm shows the change in peptide conformation.

3.3. NSP6 residues 91–112 is intrinsically disordered region in isolation and obtain helicity in the presence of membrane mimic environment and organic solvent

Circular dichroism spectroscopy was used to monitor the conformational dynamics of NSP6 (91–112). In physiological pH buffer conditions, the peptide showed strong negative ellipticity at 198 nm, characteristic of random coil conformations (Fig. 4A). Interestingly, in the presence of organic solvent (TFE) and SDS, peptide showed negative ellipticity at 208 nm and 222 nm, which showed a gain in the helical conformation of peptide (Fig. 4B & C). The results showed that the surrounding environment has a strong role in conformational dynamics of NSP6 91–112 region. Organic solvent and SDS are well-acknowledged for their hydrophobic and biological membrane mimic properties, respectively [14,15,33]. Previously, these conditions are well exploited to study the numbers of protein and peptide, under the influence of hydrophobic and membrane mimic environmental conditions. NSP6 is a transmembrane protein, and its characterized region 91–112 lies outside the membrane. So, to see the impact of membrane-mediated environment on the NSP6 91–112 region, we have used DOPS liposome. The NSP6 91–112 region acquires partial helical conformation in the presence of DOPS (Fig. 4D). Previously, Gomara et al., have performed a detailed study on association of Ebola glycoprotein fusion peptide with membranes which reveals the role of specific residues like Proline in membrane association and stable interaction of peptide [34]. Here also, it is highly possible that the outlying region of NSP6 protein may have significant role in membrane association of NSP6 protein.

Furthermore, we have used the intrinsic tryptophan present in this peptide as a fluorescence probe to monitor the tertiary structure changes in the presence of SDS and TFE (Fig. 4E & F). Trp in the presence of non-polar/hydrophobic environment gives rise to a significant blue shift [33]. Furthermore, we have observed that in the presence of TFE and SDS peptide showed blue shift, which again confirms the tertiary structural changes are happening to the peptide in these conditions and following the results obtained from the CD spectroscopy.

3.4. Temperature induces contraction in NSP6 91–112 peptide

Further, we have characterized the peptide for its structural rigidity and changes over a wide range of temperature conditions. Higher temperature conditions lead to structural changes in the peptide, related to the gain in helicity at 222 nm (Fig. 5A & B). In addition, at higher temperature, a phenomenon well described earlier is known as contraction, representing the hydrophobic forces responsible for the structural changes [15,35,36].

4. Conclusion

The protein structure determination by X-ray crystallography, NMR or Cryo-EM gives the advantage to understand the protein in an aqueous solution, which is very close to its physiological conformations. However, certain limitations still exist for a certain class of protein to be studied through these high-end techniques. In this study, we have aimed to understand the topology and 3D structure of NSP6 which is not properly determined to date despite of several advanced techniques. We have employed computer-aided protein structure determination that has been proved pivotal to understand the protein conformation and potential drug screening in current times. According to our analysis, the NSP6 protein has multiple transmembrane helical regions and two non-trans membrane regions lying in cytosolic region and ER lumen. Further, the MD simulations-based outcomes have suggested that the non-transmembrane are quiet flexible in nature which is also proved by CD and fluorescence spectroscopy-based experiments on one (residues 91–112) of the two regions. We believe, the disordered/flexible conformational dynamics of non-transmembrane regions of NSP6 protein has implications in understanding their role in protein-protein interaction and subsequent signaling events.

CRediT authorship contribution statement

Amit Kumar: conducted the experiment, acquisition and interpretation of computational data, contributed to paper writing. **Prateek Kumar:** conducted the experiment, acquisition and interpretation of computational data, contributed to paper writing. **Kumar Udit Saumya:** conducted the experiment. **Rajanish Giri:** Conceptualization, study design, Supervision, contributed to paper writing.

Declaration of competing interest

The authors declare that they have no known competing financial interests or personal relationships that could have appeared to influence the work reported in this paper.

Acknowledgments

Appendix A. Supplementary data

Supplementary data to this article can be found online at https://doi.org/10.1016/j.micpath.2021.105236.

References

[1] R. Giri, T. Bhardwaj, M. Shegane, B.R. Gehi, P. Kumar, K. Gadhave, C.J. Oldfield, V. N. Uversky, Understanding COVID-19 via comparative analysis of dark proteomes of SARS-CoV-2, human SARS and bat SARS-like coronaviruses, Cell. Mol. Life Sci. (2020).

[2] A.A.T. Naqvi, K. Fatima, T. Mohammad, U. Fatima, I.K. Singh, A. Singh, S.M. Atif, G. Hariprasad, G.M. Hasan, MdI. Hassan, Insights into SARS-CoV-2 genome, structure, evolution, pathogenesis and therapies: structural genomics approach, Biochim. Biophys. Acta (BBA) - Mol. Basis Dis. 1866 (2020) 165878.

[3] D. Bojkova, K. Klann, B. Koch, M. Widera, D. Krause, S. Ciesek, J. Cinatl, C. Münch, Proteomics of SARS-CoV-2-infected host cells reveals therapy targets, Nature 583 (2020) 469–472.

[4] D.E. Gordon, J. Hiatt, M. Bouhaddou, V.V. Rezelj, S. Ulferts, H. Braberg, A. S. Jureka, K. Obernier, J.Z. Guo, J. Batra, R.M. Kaake, A.R. Weckstein, T.W. Owens, M. Gupta, S. Pourmal, E.W. Titus, M. Cakir, M. Soucheray, M. McGregor, Z. Cakir, G. Jang, M.J. O'Meara, T.A. Tummino, Z. Zhang, H. Foussard, A. Rojc, Y. Zhou, D. Kuchenov, R. Hüttenhain, J. Xu, M. Eckhardt, D.L. Swaney, J.M. Fabius, M. Ummadi, B. Tutuncuoglu, U. Rathore, M. Modak, P. Haas, K.M. Haas, Z.Z. C. Naing, E.H. Pulido, Y. Shi, I. Barrio-Hernandez, D. Memon, E. Petsalaki, A. Dunham, M.C. Marrero, D. Burke, C. Koh, T. Vallet, J.A. Silvas, C.M. Azumaya, C. Billesbølle, A.F. Brilot, M.G. Campbell, A. Diallo, M.S. Dickinson, D. Diwanji, N. Herrera, N. Hoppe, H.T. Kratochvil, Y. Liu, G.E. Merz, M. Moritz, H.C. Nguyen, C. Nowotny, C. Puchades, A.N. Rizo, U. Schulze-Gahmen, A.M. Smith, M. Sun, I. D. Young, J. Zhao, D. Asarnow, J. Biel, A. Bowen, J.R. Braxton, J. Chen, C.M. Chio, U.S. Chio, I. Deshpande, L. Doan, B. Faust, S. Flores, M. Jin, K. Kim, V.L. Lam, F. Li, J. Li, Y.-L. Li, Y. Li, X. Liu, M. Lo, K.E. Lopez, A.A. Melo, F.R. Moss, P. Nguyen, J. Paulino, K.I. Pawar, J.K. Peters, T.H. Pospiech, M. Safari, S. Sangwan, K. Schaefer, P.V. Thomas, A.C. Thwin, R. Trenker, E. Tse, T.K.M. Tsui, F. Wang, N. Whitis, Z. Yu, K. Zhang, Y. Zhang, F. Zhou, D. Saltzberg, Q.S.B. Consortium, A. J. Hodder, A.S. Shun-Shion, D.M. Williams, K.M. White, R. Rosales, T. Kehrer, L. Miorin, E. Moreno, A.H. Patel, S. Rihn, M.M. Khalid, A. Vallejo-Gracia, P. Fozouni, C.R. Simoneau, T.L. Roth, D. Wu, M.A. Karim, M. Ghoussaini, I. Dunham, F. Berardi, S. Weigang, M. Chazal, J. Park, J. Logue, M. McGrath, S. Weston, R. Haupt, C.J. Hastie, M. Elliott, F. Brown, K.A. Burness, E. Reid, M. Dorward, C. Johnson, S.G. Wilkinson, A. Geyer, D.M. Giesel, C. Baillie, S. Raggett, H. Leech, R. Toth, N. Goodman, K.C. Keough, A.L. Lind, Z. Consortium, R.J. Klesh, K.R. Hemphill, J. Carlson-Stevermer, J. Oki, K. Holden, T. Maures, K. S. Pollard, A. Sali, D.A. Agard, Y. Cheng, J.S. Fraser, A. Frost, N. Jura, T. Kortemme, A. Manglik, D.R. Southworth, R.M. Stroud, D.R. Alessi, P. Davies, M.B. Frieman, T. Ideker, C. Abate, N. Jouvenet, G. Kochs, B. Shoichet, M. Ott, M. Palmarini, K. M. Shokat, A. García-Sastre, J.A. Rassen, R. Grosse, O.S. Rosenberg, K.A. Verba, C. F. Basler, M. Vignuzzi, A.A. Peden, P. Beltrao, N.J. Krogan, Comparative host-

coronavirus protein interaction networks reveal pan-viral disease mechanisms, Science (2020).

[5] P. V'kovski, A. Kratzel, S. Steiner, H. Stalder, V. Thiel, Coronavirus biology and replication: implications for SARS-CoV-2, Nat. Rev. Microbiol. 19 (2021) 155–170.

[6] A. von Brunn, C. Teepe, J.C. Simpson, R. Pepperkok, C.C. Friedel, R. Zimmer, R. Roberts, R. Baric, J. Haas, Analysis of intraviral protein-protein interactions of the SARS coronavirus ORFeome, PLoS One 2 (2007) e459.

[7] D. Benvenuto, S. Angeletti, M. Giovanetti, M. Bianchi, S. Pascarella, R. Cauda, M. Ciccozzi, A. Cassone, Evolutionary analysis of SARS-CoV-2: how mutation of Non-Structural Protein 6 (NSP6) could affect viral autophagy, J. Infect. 81 (2020) e24–e27.

[8] E.M. Cottam, H.J. Maier, M. Manifava, L.C. Vaux, P. Chandra-Schoenfelder, W. Gerner, P. Britton, N.T. Ktistakis, T. Wileman, Coronavirus nsp6 proteins generate autophagosomes from the endoplasmic reticulum via an omegasome intermediate, Autophagy 7 (2011) 1335–1347.

[9] M. Oostra, M.C. Hagemeijer, M. van Gent, C.P.J. Bekker, E.G. te Lintelo, P.J. M. Rottier, C.A.M. de Haan, Topology and membrane anchoring of the coronavirus replication complex: not all hydrophobic domains of nsp3 and nsp6 are membrane spanning, J. Virol. 82 (2008) 12392–12405.

[10] M.M. Angelini, M. Akhlaghpour, B.W. Neuman, M.J. Buchmeier, Severe acute respiratory syndrome coronavirus nonstructural proteins 3, 4, and 6 induce double-membrane vesicles, mBio 4 (2013).

[11] L. Schweizer, L. Mueller, Chapter 7 - protein conformational dynamics and signaling in evolution and pathophysiology, in: B.J. Arey (Ed.), Biased Signaling in Physiology, Pharmacology and Therapeutics, Academic Press, San Diego, 2014, pp. 209–249.

[12] V.N. Uversky, Intrinsically disordered proteins and their environment: Effects of strong denaturants, temperature, pH, counter ions, membranes, binding partners, osmolytes, and macromolecular crowding, Protein J. 28 (2009) 305–325.

[13] C.J. Oldfield, J. Meng, J.Y. Yang, M.Q. Yang, V.N. Uversky, A.K. Dunker, Flexible nets: disorder and induced fit in the associations of p53 and 14-3-3 with their partners, BMC Genom. 9 (Suppl 1) (2008) S1.

[14] D. Kumar, P.M. Mishra, K. Gadhave, R. Giri, Conformational dynamics of p53 N-terminal TAD2 region under different solvent conditions, Arch. Biochem. Biophys. 689 (2020) 108459.

[15] A. Kumar, P. Kumar, S. Kumari, V.N. Uversky, R. Giri, Folding and structural polymorphism of p53 C-terminal domain: one peptide with many conformations, Arch. Biochem. Biophys. 684 (2020) 108342.

[16] Bhardwaj, T., K.U. Saumya, P. Kumar, N. Sharma, K. Gadhave, V.N. Uversky, and R. Giri. Japanese encephalitis virus – exploring the dark proteome and disorder–function paradigm. *FEBS J.* n/a.

[17] W. Borchers, F.-X. Theillet, A. Katzer, A. Finzel, K.M. Mishall, A.T. Powell, H. Wu, W. Manieri, C. Dieterich, P. Selenko, A. Loewer, G.W. Daughdrill, Disorder and residual helicity alter p53-Mdm2 binding affinity and signaling in cells, Nat. Chem. Biol. 10 (2014) 1000–1002.

[18] A. Ghosh, A.S. Pithadia, J. Bhat, S. Bera, A. Midya, C.A. Fierke, A. Ramamoorthy, A. Bhunia, Self-Assembly of a 9-residue amyloid-forming peptide fragment of SARS corona virus E-protein: mechanism of self aggregation and amyloid-inhibition of hIAPP, Biochemistry 54 (2015) 2249–2261.

[19] G.M. Whitesides, J.P. Mathias, C.T. Seto, Molecular self-assembly and nanochemistry: a chemical strategy for the synthesis of nanostructures, Science 254 (1991) 1312–1319.

[20] A. Krogh, B. Larsson, G. von Heijne, E.L. Sonnhammer, Predicting transmembrane protein topology with a hidden Markov model: application to complete genomes, J. Mol. Biol. 305 (2001) 567–580.

[21] T. Nugent, D.T. Jones, Transmembrane protein topology prediction using support vector machines, BMC Bioinf. 10 (2009) 159.

[22] L. Dobson, I. Reményi, G.E. Tusnády, CCTOP: a Consensus Constrained TOPology prediction web server, Nucleic Acids Res. 43 (2015) W408–W412.

[23] P. Thévenet, Y. Shen, J. Maupetit, F. Guyon, P. Derreumaux, P. Tufféry, PEP-FOLD: an updated de novo structure prediction server for both linear and disulfide bonded cyclic peptides, Nucleic Acids Res. 40 (2012) W288–W293.

[24] Y. Shen, J. Maupetit, P. Derreumaux, P. Tufféry, Improved PEP-FOLD approach for peptide and miniprotein structure prediction, J. Chem. Theor. Comput. 10 (2014) 4745–4758.

[25] M. Källberg, G. Margaryan, S. Wang, J. Ma, J. Xu, RaptorX server: a resource for template-based protein structure modeling, Methods Mol. Biol. Clifton NJ 1137 (2014) 17–27.

[26] E.F. Pettersen, T.D. Goddard, C.C. Huang, G.S. Couch, D.M. Greenblatt, E.C. Meng, T.E. Ferrin, UCSF Chimera–a visualization system for exploratory research and analysis, J. Comput. Chem. 25 (2004) 1605–1612.

[27] J. Lee, X. Cheng, J.M. Swails, M.S. Yeom, P.K. Eastman, J.A. Lemkul, S. Wei, J. Buckner, J.C. Jeong, Y. Qi, S. Jo, V.S. Pande, D.A. Case, C.L. Brooks, A. D. MacKerell, J.B. Klauda, W. Im, CHARMM-GUI input generator for NAMD, GROMACS, AMBER, OpenMM, and CHARMM/OpenMM simulations using the CHARMM36 additive force field, J. Chem. Theor. Comput. 12 (2016) 405–413.

[28] G. Duart, M.J. García-Murria, B. Grau, J.M. Acosta-Cáceres, L. Martínez-Gil, I. Mingarro, SARS-CoV-2 envelope protein topology in eukaryotic membranes, Open Biol 10 (2002), 09.

[29] G. Duart, M.J. García-Murria, I. Mingarro, The SARS-CoV-2 envelope (E) protein has evolved towards membrane topology robustness, Biochim. Biophys. Acta BBA - Biomembr. 1863 (2021) 183608.

[30] A. Spinello, A. Saltalamacchia, A. Magistrato, Is the rigidity of SARS-CoV-2 spike receptor-binding motif the hallmark for its Enhanced infectivity? Insights from all-atom simulations, J. Phys. Chem. Lett. 11 (2020) 4785–4790.

[31] S.A. Serapian, F. Marchetti, A. Triveri, G. Morra, M. Meli, E. Moroni, G.A. Sautto, A. Rasola, G. Colombo, The answer lies in the energy: how simple atomistic molecular dynamics simulations may hold the key to epitope prediction on the fully glycosylated SARS-CoV-2 spike protein, J. Phys. Chem. Lett. 11 (2020) 8084–8093.

[32] S.A. Serapian, G. Colombo, Designing molecular spanners to throw in the protein networks, Chem. Eur J. 26 (2020) 4656–4670.

[33] A. Kumar, A. Kumar, P. Kumar, N. Garg, R. Giri, SARS-CoV-2 NSP1 C-terminal (residues 131–180) is an intrinsically disordered region in isolation, Curr. Res. Virol. Sci. 2 (2021) 100007.

[34] M.J. Gómara, P. Mora, I. Mingarro, J.L. Nieva, Roles of a conserved proline in the internal fusion peptide of Ebola glycoprotein, FEBS Lett. 569 (2004) 261–266.

[35] S. Jephthah, L. Staby, B.B. Kragelund, M. Skepö, Temperature dependence of intrinsically disordered proteins in simulations: what are we missing? J. Chem. Theor. Comput. 15 (2019) 2672–2683.

[36] M. Kjaergaard, A.-B. Nørholm, R. Hendus–Altenburger, S.F. Pedersen, F. M. Poulsen, B.B. Kragelund, Temperature-dependent structural changes in intrinsically disordered proteins: formation of α–helices or loss of polyproline II? Protein Sci. 19 (2010) 1555–1564.